ORIGINAL RESEARCH PAPER

Low temperature hydrothermal synthesis, evaluation of band gap energies and catalytic performance for Biginelli reactions of $Sr_{2-x}A_xNb_2O_{7+\delta}$ (A=Eu³⁺ and Nd³⁺) (x = 0.01 and 0.05) nanomaterials

Shahin Khademinia*, Mahdi Behzad

Department of Inorganic Chemistry, Faculty of Chemistry, Semnan University, Semnan, Iran

ABSTRACT
Nano powders Eu³⁺ and Nd³⁺ - doped $Sr_2Nb_2O_7$ were prepared by a low temperature hydrothermal method at 120 ℃ for 48 h followed by annealing at 400 °C for 3 h among $Sr(NO_3)_2$ and Nb_2O_5, Eu_2O_3 and Nd_2O_3 raw materials at stoichiometric 1:1 Sr:Nb molar ratio. Characterization of the synthesized materials was performed by X-ray powder diffraction (XRPD) technique. *FullProf* program employing profile matching with constant scale factors was employed for structural analysis. The results showed that the patterns had a main $Sr_2Nb_2O_7$ orthorhombic crystal structure with space group . FESEM images showed that the synthesized nanomaterials had flower morphologies. Ultraviolet-visible spectra analysis showed that the synthesized Eu³⁺ and Nd³⁺ - doped $Sr_2Nb_2O_7$ nanomaterials had light absorption in the ultraviolet light region. The direct optical band gap energies obtained from UV-Vis absorption spectra were 3.45, 3.50 and 3.80 eV for pure $Sr_2Nb_2O_7$, S_2 and S_4, respectively. The catalytic activity of the obtained materials in the one-pot synthesis of the heterocyclic compounds 3,4-dihydropyrimidin-2(1H)-ones (DHPMs) in Biginelli reaction is investigated. The optimized 0.03 g of the catalyst, 95 ℃ reaction temperature, and 60 min reaction time are used for the other Biginelli reactions in this work.

Keywords: *$Sr_2Nb_2O_7$, Rietveld, Hydrothermal, Crystal Structure, Biginelli.*
© 2018 Published by Journal of Nanoanalysis.

INTRODUCTION

Rare earth (RE) oxides are extensively studied in recent years because of their unique electronic, optical, and chemical properties, and their potential applications in various fields [1, 2]. The rare earth materials are used in a wide range of advanced technologies. Europium shows emission features and is used as a phosphor activation agent in colour cathode-ray tubes and in liquid-crystal flat displays [3-7]. Among many RE oxides, neodymium oxide is widely used in photonic applications [8], luminescent and thermo luminescent materials [9, 10], protective coatings [11, 12] and thin films [13]. The oxides of rare earths, including neodymium are used in important applications, such as high-efficiency phosphors and catalysts. They show good catalytic properties in several reactions, including

---

* Corresponding Author Email: shahinkhademinia@alum.semnan.ac.ir

synthesis of ammonia and oxidative coupling of methane [14-16]. There are several reports about doping metal ions into $Sr_2Nb_2O_7$ crystal system including N [17], Ba and Ta [18], La [19], Zn [20], Mo [21], Ti [22].

The Biginelli reaction is a methodology for the one-pot synthesis of 3,4-dihydropyrimidin-2-(1H)-one derivatives (DHPMs) [23,24]. DHPMs have shown biological activities [25]. Several metal oxides have been reported as nanocatalyst for the Biginelli reactions including alumina supported Mo catalysts [26], nano ZnO as a structure base catalyst [27], $MoO_3 – ZrO_2$ nanocomposite [28], $MnO_2–MWCNT$ nanocomposites [29], TiO_2 nanoparticles [30], $Mg–Al–CO_3$ and $Ca–Al–CO_3$ hydrotalcite [31], Bi_2O_3/ZrO_2 nanocomposite [32], $ZrO_2–Al_2O_3–Fe_3O_4$ [33], imidazole functionalized $Fe_3O_4@SiO_2$ [34], Alumina supported MoO_3 [35], ZrO_2-pillared clay [36], ZnO nanoparticle [37], Fe_3O_4-CNT [38], TiO_2-MWCNT [39], $Fe_3O_4@$ mesoporous SBA-15 [40], $Bi_2V_2O_7$ [41], $Bi_2Mn_2O_7$ [42], La^{3+} and Sm^{3+} doped $Bi_2Mn_2O_7$ [43], $Mn_2Sb_2O_7$ [44], and etc.

In the present work, a facile and low-temperature hydrothermal reaction is explored for the synthesis of nanostructured Eu^{3+} and Nd^{3+} doped $Sr_2Nb_2O_7$ powders using Nb_2O_5, $Sr(NO_3)_2$, Eu_2O_3, Nd_2O_3 and NaOH in the present study. To the best of our knowledge, there is no report about doping the above mentioned lanthanide ions into $Sr_2Nb_2O_7$ crystal system. Also, studying the catalytic activity of the nanomaterials in the Biginelli reactions are reported for the first time in the present work. The rietveld analysis and crystal structure investigation is used for the characterization of the obtained targets. The effect of Eu^{3+} and Nd^{3+} dopants on the morphology and optical property of the obtained materials are also studied by FESEM and UV-Vis techniques. Catalytic application of the synthesized nanomaterials was also investigated in Biginelli reactions for the synthesis of DHPMs.

EXPERIMENTAL
General remarks
All chemicals were of analytical grade, obtained from commercial sources, and used without further purification. Phase identifications were done on a powder X-ray diffractometer D5000 (Siemens AG, Munich, Germany) using CuKα radiation. Field emission scanning electron microscope (Hitachi FE-SEM model S-4160) was used to examine the morphology of the obtained materials. Philips

XL30 scanning electron microscope (Philips, Amsterdam, Netherlands) equipped with energy-dispersive X-ray (EDX) spectrometer was employed for studying the elemental analyses of the obtained materials. Absorption spectra were recorded on Analytik Jena Specord 40 (Analytik Jena AG Analytical Instrumentation, Jena, Germany). The purity of products was checked by thin layer chromatography (TLC) on glass plates coated with silica gel 60 F254 using a 6:4 volumetric ratio of n-hexane:ethyl acetate mixture as mobile phase and comparison of melting points with authentic samples. Melting points were obtained on a thermoscientific 9100 apparatus.

MATERIALS PREPARATION
Synthesis of Nd^{3+} - doped $Sr_2Nb_2O_7$
The synthesis procedure is according to our previously reported work [45]. For the synthesis of the targets, 0.20 g (0.752 mmol) of Nb_2O_5 (Mw = 265.82 gmol⁻¹), 0.158 g (0.747 mmol) or 0.156 g (0.737 mmol) of $Sr(NO_3)_2$ (Mw = 211.62 gmol⁻¹) and 0.0034 g (0.01 mmol) (S_1) or 0.0017 g (0.05 mmol) (S_2) of Nd_2O_3 (Mw= 336.48 gmol⁻¹) were added into 50 mL of hot aqueous solutions of 2 M NaOH under magnetic stirring at 80˚C, respectively. The resulting solution was stirred for 15 min. Then the obtained solution was transferred into a 100-mL Teflon lined stainless steel autoclave. The autoclave was sealed and treated thermally at 120˚C for 48 h in an oven. When the synthesis process was completed, the autoclave was cooled to room temperature by quenching in water immediately. The prepared powder was washed with distilled water for and dried at 110˚C for 20 min under normal atmospheric condition. The prepared powder was then transferred in a crucible and treated thermally again in a one step at 400˚C for 3h in a furnace. After the desired time, the crucible was allowed to cool down normally to room temperature.

Synthesis of Eu^{3+}-doped $Sr_2Nb_2O_7$
In another typical synthetic experiment, 0.20 g (0.752 mmol) of Nb_2O_5 (Mw = 265.82 gmol⁻¹), 0.158 g (0.747 mmol) or 0.156 g (0.737 mmol) of $Sr(NO_3)_2$ (Mw = 211.62 gmol⁻¹) and 0.00352 g (0.01 mmol) (S_3) or 0.00176 g (0.05 mmol) (S_4) of Eu_2O_3 (Mw= 351.92 gmol⁻¹) were added to 50 mL of hot aqueous solutions of 2 M NaOH under magnetic stirring at 80˚C, respectively. The resulting solution was stirred for 15 min. Then it was transferred to a

100-mL Teflon lined stainless steel autoclave. The autoclave was sealed and heated at 120˚C for 48 h in an oven. When the desired reaction was completed, the autoclave was cooled to room temperature by quenching in water, immediately. The prepared powder was washed with distilled water and dried at 110˚C for 20 min under normal atmospheric condition. The obtained dried powder was treated thermally in a one step at 400˚C for 3h in a furnace. When the desired time has elapsed, the furnace was shut down and allowed to cool down normally to room temperature.

General procedure for the synthesis of DHPMs

In a typical procedure [42-44], a mixture of aldehyde (1 mmol), ethyl acetoacetate (1 mmol), urea (1.2 mmol) and 0.03 g ($\approx 8.3 \times 10^{-2}$ mmol) of $Sr_2Nb_2O_7$ or Eu^{3+} and or Nd^{3+} doped $Sr_2Nb_2O_7$ (Mw ≈ 361 gmol^{-1}) as catalyst were placed in a round-bottom flask under solvent free conditions. The suspension was stirred at 95°C. The reaction was monitored by thin layer chromatography (TLC) [6:4 n-hexane:ethyl acetate]. After completion of the reaction, the solid crude product was washed with deionized water to separate the unreacted raw

materials. The remaining solid was then dissolved in ethanol to separate the heterogeneous catalyst. The solid catalyst was washed with acetone and dried in oven at 90˚C to be used in the next cycles. The ethanolic solution was evaporated to dryness to obtain the target DHPMs.

Characterization

Figure 1 shows the XRPD analysis of the doped $Sr_2Nb_2O_7$ samples obtained in the θ-2θ geometry with Cu-Kα radiation. Structural analysis is done by the *FullProf* program by employing profile matching with the constant scale factor. The blue bars show the Bragg positions of the main phase $Sr_2Nb_2O_7$. The red bars show the Bragg positions of the impurity phase Nb_2O_5 (JCPDS no: 00-030-873). The results showed that the patterns had a main $Sr_2Nb_2O_7$ crystal structure with space group *Cmc21*. The data show that doping process has an influence on the crystal growth and purity of the obtained materials. It can also been found that the other crystallographic parameters such as interplanar spacing, crystallite size, dislocation density and strain values are affected by changing and increasing the dopant amounts.
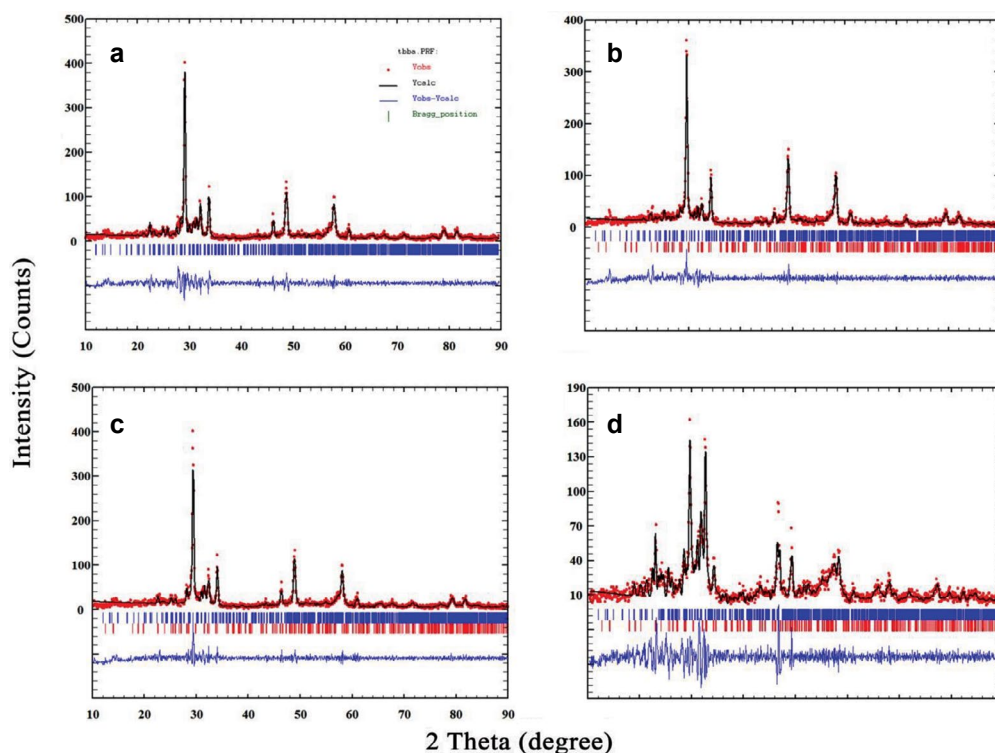
Fig. 1. XRPD patterns of the synthesized Nd^{3+} and Eu^{3+}doped $Sr_2Nb_2O_7$ nanomaterials and the rietveld analyses. Where (a) is S_1, (b) is S_2, (c) is S_3 and (d) is S_4.

Rietveld analyses data of the obtained samples are summarized in table 1. The values of R_{Bragg}, R_F and χ^2 show that the analyses are well. The data show that increasing the crystal phase purity has a considerable effect on the goodness of the refinement. So, the refinement for S_1 and S_3 was performed better than those for S_2 and S_4. Besides, the phase purity value of the obtained materials shows that the parameter was decreased with increase the dopant amount in the crystal system. This can be due to the difference between the ionic radii of the dopant amount and strontium ion, causes a disorder in the unit cell when a considerable amount of the dopant incorporates in the unit cell cavity. Also, the crystal phase growth was studied by investigating the counts value of the sharpest peak in the XRPD pattern. It was found that the value was decreased with increasing the dopant amount in the crystal system. The disorder, mentioned above, can be responsible for the phenomenon. However, there is another parameter that is the difference charge between dopant and Sr^{2+}. The difference creates another deficiency in the crystal system due to the deviation of the stoichiometry of oxygen in $A_2B_2O_7$ formula. The experimental observations indicate the more the deviation the less the crystal growth and purity.

Table 1. Quantitative phase analysis for doped - $Sr_2Nb_2O_7$ nano-materials

Sample	Rietveld parameters			Phase purity (%)	Counts
	R_{Bragg}	R_F	χ^2		
S_1	2.12	1.05	1.73	100	407
S_2	1.36	0.74	1.63	88	366
S_3	1.37	0.802	1.74	91	408
S_4	0.899	2.11	1.58	66	164

Table 2 shows the lattice parameters of the obtained targets. The data also show the unit cell volume of the samples calculated by formula 1. It shows that the volume of the samples is decreased with increasing the dopant amount in the crystal system. The data show that the decreasing in the unit cell volume for Eu^{3+} doped $Sr_2Nb_2O_7$ is larger than that for Nd^{3+} doped $Sr_2Nb_2O_7$. This is due to the smaller ionic radii of Eu^{3+} (1.07 Å) compared to Nd^{3+} (1.12 Å).

Table 2. Lattice parameters data for pure and doped - $Sr_2Nb_2O_7$ nanomaterials

Sample	a (Å)	b (Å)	c (Å)	Volume (Å³)
S_1	3.91127	26.72003	26.72003	2792
S_2	3.82528	26.55433	26.55433	2697
S_3	3.86266	26.63212	26.63212	2739
S_4	3.80668	26.60026	26.60026	2693

Interplanar spacing (d) data of the obtained nanomaterials are summarized in table 3. The d parameter data were calculated by Bragg's equation and formula (2). The obtained data are in good consistency with each other. It was found that the d parameter values were decreased by doping the lanthanide ions into the crystal system. It is due to the substitution of Sr^{2+} (1.26 Å) by Nd^{3+} (1.12 Å) and Eu^{3+} (1.07 Å) with smaller ionic radii. So there is a contraction in the unit cell with doping the lanthanide ions into $Sr_2Nb_2O_7$ crystal system.

Table 3. Interplanar spacing (d) data for pure and doped - $Sr_2Nb_2O_7$ nanomaterials.

Pure $Sr_2Nb_2O_7$	S_1	S_2	S_3	S_4
d_{Bragg} (Å) 3.902	3.0473	3.0335	3.0551	3.0522
$d_{cal.}$ (Å) 3.600	3.0717	3.0225	3.0442	3.0152
2θ (°) 22.77	29.28	29.42	29.21	29.24

The crystallographic data of the obtained samples were calculated and compared to the observed data. The unit cell volume can be obtained from the bellow formula:

$$V = a.b.c \qquad (1)$$

Where a, b and c are the lattice parameters and V is the cell volume.

The interplanar spacing is calculated by the following formula:

$$1/d^2 = h^2/a^2 + k^2/b^2 + l^2/c^2 \qquad (2)$$

With using the peak with maximum intensity at 29.4 °, with the (h k l) value of (152), the relation is as below:

$$1/d^2 = 1/a^2 + 25/b^2 + 4/c^2$$

Table 4 shows the crystallite sizes, dislocation density

and strain date of the as-synthesized nanomaterials in different dopant concentrations calculated via Scherrer equation:

$$D=k\lambda/(B1/2 \cos\theta) \qquad (3)$$

In this equation, D is the entire thickness of the crystalline sample, λ is the X-ray diffraction wavelength (0.154 nm), and k is the Scherrer constant (0.9), $B_{1/2}$ of FWHM is the full width at half its maximum intensity and θ is the half diffraction angle at which the peak is located. The crystallite size data mentioned in table 4 show that the values were increased compared to pure $Sr_2Nb_2O_7$ nanomaterial with doping Eu^{3+} into $Sr_2Nb_2O_7$. It was also found that with doping Nd^{3+} into $Sr_2Nb_2O_7$, the calculated crystallite sizes were decreased to the value nearly equal to the pure $Sr_2Nb_2O_7$.

The value of the dislocation density (δ) which is related to the number of defects in the crystal was calculated from the average values of the crystallite size (D) by the relationship given below:

$$\delta=1/D^2 \qquad (4)$$

It was found that the dislocation density was decreased when doping the dopant ions in the crystal system. The behavior is due to the changing the crystallite sizes of the materials with doping the lanthanide ions in $Sr_2Nb_2O_7$ crystal structure.

The strain (ε) values were determined with the use of the following formula:

$$\varepsilon=(\beta_{hkl} \cos\theta)/4 \qquad (5)$$

The variation in the strain as a function of doping processes is included in table 4. The decreasing in the strain with doping and increasing the dopants amounts is probably due to the enhancement in the degree of crystallite of the obtained target.

Elemental analysis

Figure 3 (a and b) shows the EDX spectra of the obtained nanomaterials as a function of Nd_2O_3 and Eu_2O_3 concentrations. The spectra indicated that the X-rays emitted from various elements. The peaks corresponded to Nd, Eu, Sr, Nb, and O atoms present in the samples are labeled. The respective energy positions and the specific X-ray lines from various elements are also indicated. The figure illustrates the EDX analyses for the samples doped theoretically with 0.05 mmol of Nd_2O_3 and Eu_2O_3 into the crystal system which verify the doping and the compositional analysis of Eu^{3+} and Nd^{3+} in $Sr_2Nb_2O_7$. The normalized elemental analyses of the doped materials showed that the experimental formulas were $Sr_{1.96}Nd_{0.04}Nb_2O_7$ and $Sr_{1.963}Eu_{0.037}Nb_2O_7$.

Table 4. Scherrer data information for pure and doped - $Sr_2Nb_2O_7$ nanomaterials

Sample	2θ	θ value	$B_{1/2}$ (°)	$B_{1/2}$ (rad)	$\cos\theta_B$	D (nm)	δ(lines/m²)	ε
$Sr_2Nb_2O_7$	22.73	11.365	0.3000	0.005200	0.980390	27.18	13.5	1.27
S_1	29.28	14.64	0.2558	0.004462	0.96753	32.10	9.7	1.08
S_2	29.42	14.71	0.2558	0.004462	0.96722	32.12	9.7	1.08
S_3	29.21	14.61	0.2558	0.004462	0.96769	32.10	9.7	1.08
S_4	29.24	14.62	0.2558	0.004462	0.96762	32.10	9.7	1.08
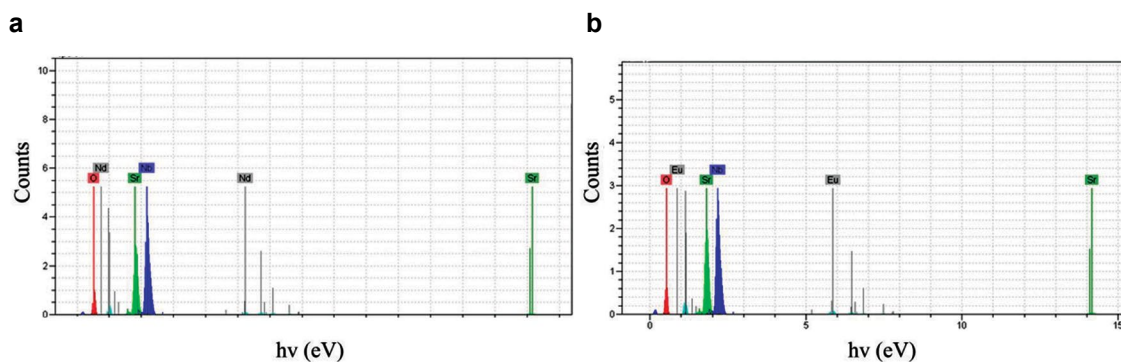
Fig. 2. Elemental analyses data for a) S_2 and b) S_4.

Morphology analysis

Figure 3 shows the FESEM images of S_1 and S_2. Figure 3 a and b shows the FESEM images of S_1. It was found that the morphology of the obtained material was flower. However, it indicated that the flower was composed of rod structures which join together in a point and make a flower structure. Figure 3 b shows that the thickness size of the rods is about 80 - 100 nm. Figure 3 c and d shows the FFESEM images of S_2. It shows that the morphology is changed when the dopant amount is increased. It shows that there are two types of flower morphology. One type is formed from rod structures. The second type is formed by joining plate structures to each other. It was found that the thickness size of the plates was about 30 - 40 nm.

Figure 4 a and b shows the FESEM images of S_3. Figure 4 a indicates that the size and morphology of the obtained target are homogeneous. Besides, figure 4 b shows that the morphology of the material is flower formed by crossing rods to each other. The thickness size of the rods is about 100 - 120 nm. Figure 4 c and d shows the FESEM images of S_4. The figure indicates that the rod-formed flower structure has been changed to the rods with heterogeneous morphology. The thickness size of the rods is about 100 - 120 nm. Figure 4 d shows that the morphology of the target was changed to the plate-formed flower with increasing the dopant amount. It is found that the plate thickness size is about 30 - 40 nm.
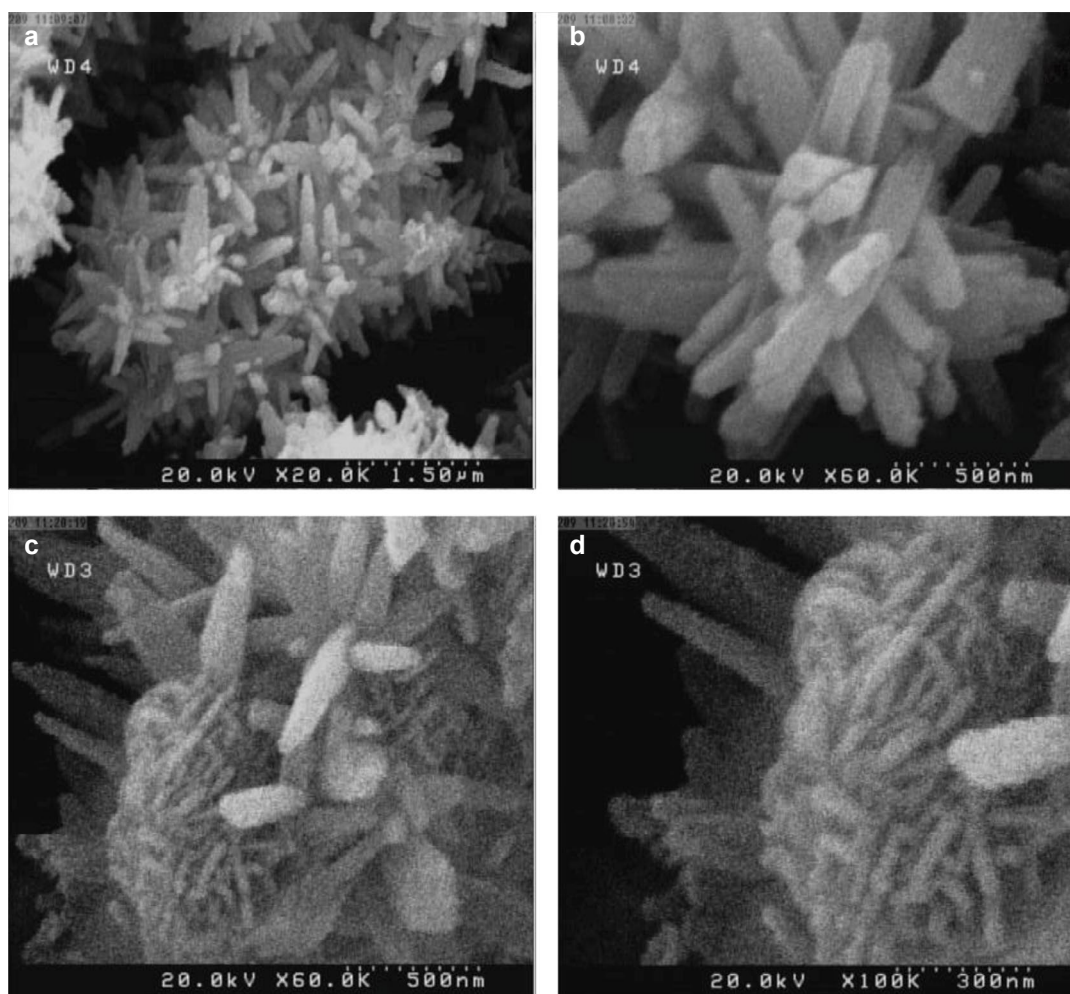
Fig. 3. FESEM images of S_1 and S_2.
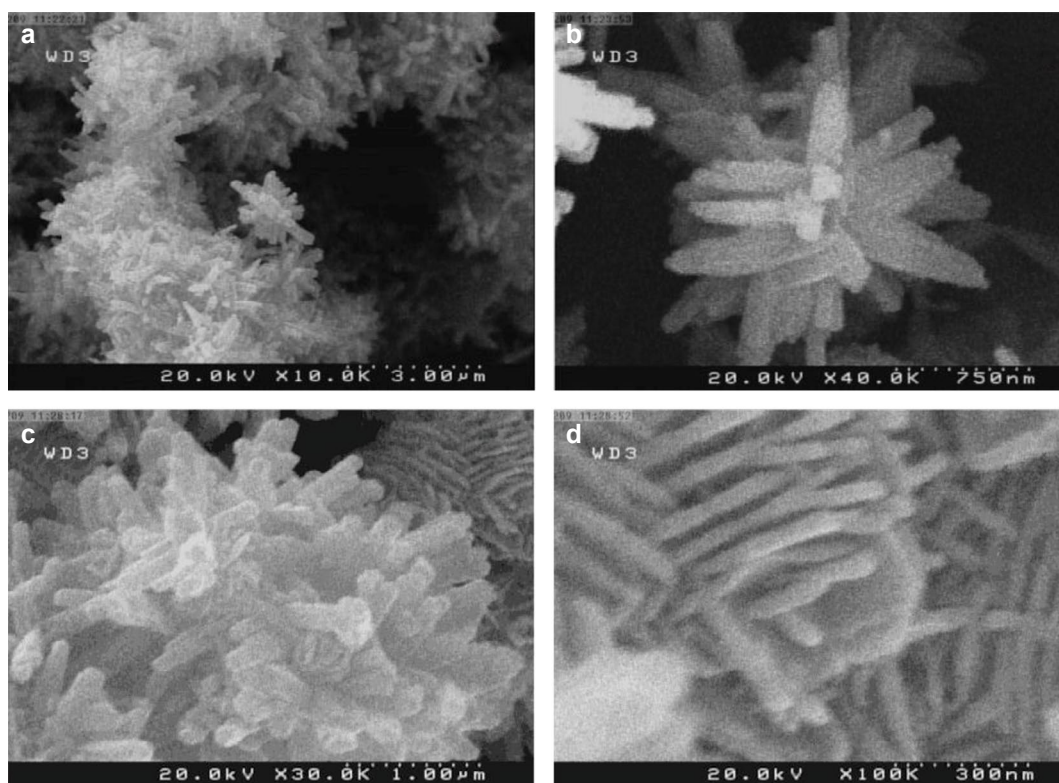
Fig. 4. FESEM images of S_3 and S_4.

The direct optical band gap energies of the pure and doped $Sr_2Nb_2O_7$ nanomaterials obtained from UV-Vis absorption spectra are shown in figure 5. According to the results of Pascual et al. [46], the relation between the absorption coefficient and incident photon energy can be written as $(\alpha h\nu)^2 = A(h\nu - E_g)$, where A and E_g are a constant and the direct band gap energy, respectively. The bandgap energies were evaluated from extrapolating the linear part of the curve to the energy axis. It was found that the direct optical band gaps were 3.45, 3.50 and 3.85 for pure $Sr_2Nb_2O_7$, S_2 and S_4, respectively. The data show that increasing the dopant amount increased the direct optical band gaps of the targets. Increasing the optical band gap can be due to the decreasing the unit cell volume and lanthanide contraction effect.

Catalytic studies
Biginelli reaction for the synthesis of DHPMs
The direct synthesis involves the condensation between ketoesters, aldehydes, and ureas in the presence of either Lewis or mineral acids. DHPMs were prepared by the reaction of aromatic aldehyde,

ethyl acetoacetate and urea with 8.3×10^{-2} mmol of each of the obtained samples at 95 °C for 60 min under solvent-free conditions (Scheme 1). Several parameters affecting the catalytic reactions were analysed and optimized.
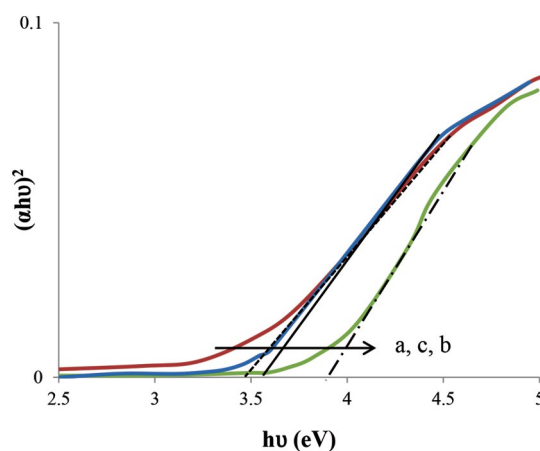
Fig. 5. Plots of Plots of $(\alpha h\nu)^2$ versus $h\nu$ (eV) for a) Pure $Sr_2Nb_2O_7$, b) S_2 and c)S_4.

Effect of different parameters on the catalytic reaction

Different parameters such reaction time, temperature and the amount of the nanocatalyst were optimized on the catalytic reaction using benzaldehyde as the aldehyde derivative. Table 5 shows the effect of the different parameters on the reaction efficiency. It was found that the efficiency was increased with increasing the amount of the nanocatalyst from 0.02 to 0.03; however by changing its amount over 0.04 g, the efficiency was decreased. So, we found that the optimal amount of the nanocatalyst was 0.03 g. The effect of temperature on the reaction was also investigated using the optimized amount of the catalyst. According to the table 5, it was found that the reaction efficiency was increased with increasing the temperature from 70 to 95 °C but over the temperature, the efficiency maintained nearly constant. Hence, the optimal temperature for the reaction was found to be 95 °C. Table 5 also shows that the efficiency of the synthesis procedure was increased with increasing the reaction time from 50 to 60 min and the efficiency maintained constant with increasing the reaction time. So, 0.03 g of the catalyst, 95 °C reaction temperature, and 60 min reaction time were used for the other Biginelli reactions in this work.

derivatives and the results are collected in table 6. The data showed that doping the lanthanide ions changed the activity and so the catalytic performance of the obtained materials. It was found that when the doping the cations into the crystal system, the performance was increased for the derivative 2-Cl and 4-Cl benzaldehyde derivatives. The catalytic data indicate that the hard/soft nature of the cations play a more important role in the catalytic performance for the Biginelli reactions when an electron withdrawing substituent agent as the benzaldehyde derivative is used in replace of benzaldehyde agent. Scheme 1 shows a summary of the reaction pathway.
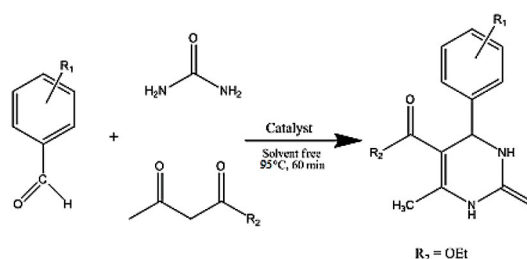
Scheme. 1. Schematic representation of the reaction pathway for the synthesis of DHPMs.

Table 5. Optimization of the different conditions for the synthesis of DHPMs

Amount of catalyst (g)	Time (min)	Temperature (°C)	Yield (%)
0.02	60	80	64
0.02	60	95	70
0.02	70	95	70
0.03	50	70	62
0.03	60	80	77
0.03	60	95	80
0.03	70	95	82
0.04	50	70	58
0.04	60	80	65
0.04	70	80	68
0.04	60	95	65
0.04	70	95	72

Table 6. Biginelli reactions using ethyl acetoacetate and urea with different benzaldehyde derivatives.

Sample	Band gap (eV)	Yield (%)		
		H	4- Cl	2- Cl
S$_1$	3.45	80	86	91
S$_2$		80	85	92
S$_3$	3.50	77	68	95
S$_4$		73	98	78
S$_5$	3.85	65	92	81

The optimized parameters from the previous section were used for the synthesis of other

To show the merit of the present work, we have compared the obtained nanocatalysts results with some of the previously reported catalysts in the synthesis of DHPMs (Table 7). It is clear that the synthesized nanomaterials showed greater activity than some other heterogeneous catalysts. It is clear that the present conditions for the synthesis of DHPMs is more facile and the yields of the obtained materials under the present conditions are comparable with those of the catalysts applied at sever catalytic conditions including at higher reaction temperature, using reflux and reaction solvent.

Table 7. Comparison study of the catalytic ability of the synthesized $Bi_2Mn_2O_7$ with other catalysts

Catalyst	R_1	Catalyst amount	Reaction Condition	Yield %	Time (min)	Ref.
$Sr_2Nb_2O_7$	H	0.03 g	solvent-free, 95°C	80	60	This work
	4-Cl	0.03 g		86		
	2-Cl	0.03 g		91		
Eu^{3+}-doped $Sr_2Nb_2O_7$	H	0.03 g	solvent-free, 95°C	80	60	This work
	4-Cl	0.03 g		85		
	2-Cl	0.03 g		92		
Nd^{3+}-doped $Sr_2Nb_2O_7$	H	0.03 g	solvent-free, 95°C	73	60	This work
	4-Cl	0.03 g		98		
	2-Cl	0.03 g		78		
$Mn_2Sb_2O_7$	H	0.04 g	solvent-free, 103°C	81	62	[37]
	4-Cl			92		
	2-Cl			77		
La^{3+}-doped $Bi_2Mn_2O_7$	H	0.014 g	solvent-free, 104°C	92	66	[36]
	4-Cl			51		
	2-Cl			78		
Sm^{3+}-doped $Bi_2Mn_2O_7$	H	0.014 g	solvent-free, 104°C	82	66	[36]
	4-Cl			37		
	2-Cl			71		
$Bi_2Mn_2O_7$	H	2.2×10^{-2} mmol	solvent-free, 104°C	96	66	[35]
	4-Cl			89		
	2-Cl			86		
$Mo/\gamma - Al_2O_3$	H	0.3 g	solvent-free, 100°C	80	60	[28]
Bi_2O_3/ZrO_2	H	20 mol%	solvent-free, 80-85 °C	85	120	[31]
	4-Cl			85	120	
	2-Cl			82	165	
$ZrO_2–Al_2O_3–Fe_3O_4$	H	0.05 g	Ethanol, reflux, 140 °C	82	300	[32]
	4-Cl			66		
	2-Cl			40		
$Bi_2V_2O_7$	H	3.1×10^{-2} mmol	solvent-free, 90°C	89	60	[34]
	4-Cl			92		
	2-Cl			98		
ZnO	H	25 mol%	solvent-free, 90°C	92	50	[38]
	4-Cl			95		

CONCLUSION

In this his work, Nd^{3+} and, Eu^{3+} doped $Sr_2Nb_2O_7$ nanomaterials were synthesized via hydrothermal method followed by annealing at 400 °C for 3 h. Structural analyses were performed by FullProf program employing profile matching. The data showed that the syntheses were successful and the patterns had a main $Sr_2Nb_2O_7$ orthorhombic crystal structure with space group Cmc21. The crystallographic data of the obtained materials such interplanar spacing, crystallite size, crystal phase growth and purity, dislocation density and strain values were investigated and related to the type and amount of the dopant ion. FESEM images showed the flower structure in the as-synthesized materials. Direct band gap energy was evaluated by extrapolating the linear part of the curve to the energy axis. It was found that the band gaps were increased with doping Nd^{3+} and Eu^{3+} into $Sr_2Nb_2O_7$ crystal system. The catalytic data indicated that the hard/soft nature of the cations played a more important role in the catalytic performance for the Biginelli reactions when an electron withdrawing substituent agent as the benzaldehyde derivative was used in replace of benzaldehyde agent.

CONFLICT OF INTEREST

The authors declare that there is no conflict of interests regarding the publication of this manuscript.

REFERENCE

1. T. Tago, S. Tashiro, Y. Hashimoto, K. Wakabayashi, M. Kishida, J. Nanoparticle Res., 5, 55 (2003).
2. Y. Castro, B. Julian, C. Boissi`ere, B. Viana, H. Amenitsch, D. Grosso, C. Sanchez, Nanotech., 18, 055705 (2007).
3. T. Yan, D. Zhang, L. Shi, H. Li, J. Alloys Compd., 487, 483 (2009).
4. F.W.B. Lopes, C.P. de Souza, A.M.V. de Morais, J.P. Dallas, J.R. Gavarri, Hydrometallurgy., 97, 167 (2009).
5. Y. Li, M. Ge, J. Li, J. Wang, , H. Zhang, Cryst. Eng. Comm., 13, 637 (2011).
6. A. Hadi, I.I. Yaacob, Mater. Lett., 61, 93 (2007).
7. Z.S. Xiao, B. Zhou, , F. Xu, F. Zhu, L. Yan, F. Zhang, A.P. Huang, Phys. Lett. A., 373, 890 (2009).
8. T. Sreethawong, S. Chavadej, S. Ngamsinlapasathian, S. Yoshikawa, Solid State Sci., 10, 20 (2008).
9. R. Bazzi, M.A. Flores-Gonzalez, C. Louis, K. Lebbou, C. Dujardin, A. Brenier, W. Zhang, O. Tillement, E. Bernstein, P. Perriat, J. Lumin., 102, 445 (2003).
10. C. Soliman, Nucl. Instrum. Methods Phys. Res., Sect. B., 251, 441 (2006).
11. M. Zawadzki, L. Kepi, J. Alloys Compd., 380, 255 (2004).
12. B. Zhaorigetu, R. Ga, M. Li, J. Alloys Compd., 427, 235 (2007).
13. A. Kosola, J. Päiväsaari, M. Putkonen, L. Niinistö, Thin Solid Films., 479, 152 (2005).
14. Y, Kadowakim, K. Aika, J. Catal., 161, 178 (1996).
15. M.R. Lee, M.-J. Park, W. Jeon, J.-W. Choi, Y.-W. Suh, D.J. Suh, Fuel Proc. Tech., 96, 175 (2012).
16. S.A. Osseni, Y.G. Denisenko, J.K. Fatombi, E.I. Sal'nikova, O.V. Andreev, J. Nanostruct. Chem., https://doi.org/10.1007/s40097-017-0243-4.
17. S.M. Ji, P.H. Borse, H.G. Kim, D.W. Hwang, J.S. Jang, S.W. Bae, J.S. Lee, Phys. Chem. Chem. Phys., 7, 1315 (2005).
18. G. Chen, C.W. Gong, C.L. Fu, X.D. Peng, W. Cai, R.L. Gao, X.L. Deng, Mater.Sci. Forum., 815, 125 (2015).
19. B. Brahmaroutu, G.L. Messing, S. Trolier-McKinstry, J. Mater. Sci., 35, 5673 (2000).
20. J.P. Zou, D.D. Wu, S.K. Bao, J. Luo, X.B. Luo, S.L. Lei, H.L. Liu, H.M. Du, S.L. Luo, C.T. Au, S.L. Suib, *ACS Appl. Mater. Interfaces.*, 7, 28429 (2015).
21. J. Nisar, B. Pathak, R. Ahuja, Appl. Phys. Lett., 100, 181903 (2012).
22. J.Y.Yu, http://ir.lib.ksu.edu.tw/handle/987654321/26660.
23. P. Biginelli, Ber. Dtsch. Chem. Ges., 24, 1317 (1891).
24. E. Kolvari, N. Koukabi, M. M. Hosseini. J. Mol. Catal. A: Chem., 397, 68 (2015).
25. K. Singh, D. Arora, S. Singh, Mini Rev. Med. Chem., 9, 95 (2009).
26. K. Kouachi, G. Lafaye, S. Pronier, L. Bennini, S. Menad, J. Mol. Catal. A: Chem., 395, 210 (2014).
27. F. Tamaddon, S. Moradi, J. Mol. Catal. A: Chem., 370, 117 (2013).
28. S. Samantaray, B.G. Mishra, J. Mol. Catal. A: Chem., 339, 92 (2011).
29. J. Safari, S. G. Ravandi, J. Mol Catal. A: Chem., 373, 72 (2013).
30. H.R. Memarain, M. Ranjbar, J. Mol. Catal. A: Chem., 356, 46 (2012).
31. J. Lal, M. Sharma, S. Gupta, P. Parashar, P. Sahu, D.D. Agarwal, J. Mol. Catal. A: Chem., 352, 31 (2012).
32. V.C. Guguloth, G. Raju, M. Basude, S. Battu, Inter. J. Chem. Anal. Sci., 5, 86 (2014).
33. A. Wang, X. Liu, Z. Su, H. Jing, Catal. Sci. Technol., 4, 71 (2014).
34. J. Javidi, M. Esmaeilpour, F.N. Dodeji, RSC Adv., 5, 308 (2015).
35. S.L. Jian, V.V.D.N. Prasad, B. Sain, Cat. Com., 9, 499 (2008).
36. V. Singh, V. Sapehiyia, V. Srivastava, S. Kaur. Catal. Com., 7, 571 (2006).
37. Kh. Pourshamsian. Int. J. Nano Dimens., 6, 99 (2015).
38. J. Safari, S.G. Ravandi, RSC Adv.,4, 11486 (2014).
39. J. Safari, S.G. Ravandi, New J. Chem.,38, 3514 (2014).

40. J. Mondal, T. Sen, A. Bhaumik, Dalton Trans., 41, 6173 (2012).

41. S. Khademinia, M. Behzad, H. S. Jahromi, RSC Adv., **5**, 24313 (2015).

42. S. Khademinia, M.Behzad, A. Alemi, M. Dolatyarim, S. M. Sajjadi, RSC Adv., 5, 71109 (2015).

43. S. Khademinia, M. Behzad, J. Nanostruct., (in press).

44. S. Khademinia, M. Behzad, M. Rahimkhani, Chem. Solid Mater., 2, 79 (2015).

45. S. Khademinia, M. Behzad, Adv. Powder Tech., 26, 644 (2015).

46. J. Pascual, , J. Camassel, , M. Mathieu, Phys. Rev. B., 18, 5606 (1978).

47. Kh Pourshamsian, Int. J. Nano Dimens., 6, 99 (2015).